

1 **Bisphenol A alters cellular microenvironment to promote survival after oxidative stress**

2 Natalie R. Gassman¹, Erdem Coskun^{2,3}, Pawel Jaruga², Miral Dizdaroglu² and Samuel H.
3 Wilson^{1*}

4 ¹Genome Integrity and Structural Biology Laboratory, NIEHS, National Institutes of Health, 111
5 T.W. Alexander Drive, Research Triangle Park, NC 27709, USA.

6 ²Biomolecular Measurement Division, National Institute of Standards and Technology,
7 Gaithersburg, MD 20899, USA.

8 ³Faculty of Pharmacy, Gazi University, Ankara, Turkey

9

10 * To whom correspondence should be addressed:

11 Samuel H. Wilson, Genome Integrity and Structural Biology Laboratory, National Institute of
12 Environmental Health Sciences, National Institutes of Health, P.O. Box 12233, Research
13 Triangle Park, NC 27709-12233

14 E-mail: wilson5@niehs.nih.gov

15 Telephone: 919-541-4701

16 Fax: 919-541-4724

17

18 **Short title:** BPA alters cellular microenvironment

19 **Acknowledgements**

20 We thank the NIEHS Microarray Core (Dr. Kevin Gerrish, Joetta Hitchcock-Smith, and Liwen
21 Liu) and Dr. Carl Bortner and Maria Sifre for their assistance with flow cytometry

22 measurements. This research was supported by Research Project Numbers Z01-ES050158 and

23 Z01-ES050159 in the Intramural Research Program of the National Institutes of Health, National

24 Institute of Environmental Health Sciences. NRG is funded by 1K99ES023813-01. The funders
25 had no role in study design, data collection and analysis, decision to publish, or preparation of
26 the manuscript. Certain commercial equipment or materials are identified in this paper in order to
27 specify adequately the experimental procedure. Such identification does not imply
28 recommendation or endorsement by the National Institute of Standards and Technology, nor
29 does it imply that the materials or equipment identified are necessarily the best available for the
30 purpose.

31

32 **Competing interests:** The authors have declared that no competing interests exist.

33 **Abstract**

34

35 **Background:** Exposure to bisphenol A (BPA) has been reported to alter global gene expression,
36 induce epigenetic modifications, and interfere with complex regulatory networks of cells. In
37 addition to these reprogramming events, we have demonstrated that BPA exposure generates
38 reactive oxygen species and promotes cellular survival when co-exposed with dietary oxidizing
39 agent potassium bromate (KBrO₃).

40 **Objectives:** To determine the cellular microenvironment changes induced by BPA co-exposure
41 that promoted cell survival and to determine if these changes were unique to co-exposure.

42 **Methods:** Ku70-deficient cells were exposed to BPA, KBrO₃, and co-exposed with both agents.
43 4 and 24 h post-damage initiation, we performed whole genome microarray analysis and
44 evaluated chromatin structure, DNA lesion load, glutathione content, and intracellular pH.

45 **Results:** We found that 4 h post-damage initiation BPA co-exposure suppressed DNA repair by
46 condensing chromatin and reducing transcription of DNA repair proteins. BPA also stabilized
47 the intracellular pH change observed after KBrO₃ treatment. 24 h post-damage initiation, BPA
48 exposed cells showed less condensed chromatin; oxidatively induced DNA lesions were reduced
49 compared to 4 h; intracellular glutathione was slightly depleted; intracellular pH was reduced,
50 while KBrO₃ showed an increased pH; and significant up-regulation in DNA repair proteins was
51 observed for the co-exposure condition.

52 **Conclusion:** These results support the induction of an adaptive response by BPA co-exposure
53 that delays the repair of oxidatively induced DNA lesions. Further work is required to understand
54 the long-term consequences of this delayed repair; however, this study demonstrates that BPA
55 exposure significantly alters the cellular microenvironment to promote survival.

56 **Keywords:** adaptive response, bisphenol A, DNA damage, DNA repair, endocrine disruptor,
57 oxidative stress, oxidatively induced DNA lesions, potassium bromate

58

59 **Introduction**

60 World-wide production of bisphenol A (BPA) has increased exponentially as the demand for this
61 chemical in consumer products, from food and beverage containers to epoxies, has grown
62 (Vandenberg et al. 2007). This increase has resulted in elevated BPA levels in the air, water, soil,
63 and also in human samples (Vandenberg et al. 2007; Vandenberg et al. 2010). The ubiquity of
64 BPA in our environment has resulted in concurrent exposures of BPA with endogenous and
65 exogenous DNA damaging events. Together these exposures can increase the damage load of
66 genomic DNA and have implications for genomic stability and the development and progression
67 of disease. While, the estrogenic properties of BPA are one source of concern, BPA exposure has
68 been shown to cause DNA damage independent of its estrogenic properties (Iso et al. 2006;
69 Nishimura et al. 2014b; Tiwari et al. 2012; Wu et al. 2013; Yang et al. 2009), yet how the DNA
70 damage response and repair pathways address BPA exposure has not been extensively
71 investigated.

72

73 We have demonstrated that exposure to BPA generates reactive oxygen species (ROS) in a model
74 experimental system of Ku70-deficient mouse embryonic fibroblast (MEF) (Gassman et al.
75 2015). The Ku70-deficient cell line is sensitive to oxidizing agents, and its deficiency in double-
76 strand break repair by non-homologous end joining, which also serves as a back-up repair
77 pathway for the base excision repair (BER) pathway, provides a window into the cellular
78 responses to oxidatively induced DNA damage (Choi et al. 2014; Li et al. 2013). Using this

79 repair deficient cell line, BPA exposure was found to increase oxidatively induced DNA lesions
80 in the genomic DNA (Gassman et al. 2015). Since these BPA-induced DNA lesions would occur
81 in concert with other DNA damaging events during environmental exposures, the effects of co-
82 exposure of BPA with the dietary oxidizing agent, potassium bromate (KBrO_3) were also
83 examined. KBrO_3 -induced ROS and oxidatively induced DNA lesions, and co-exposure to both
84 BPA and KBrO_3 resulted in a further increase in the levels of oxidatively induced DNA lesions
85 (Table 1), particularly in that of 2,6-diamino-4-hydroxy-5-formamidopyrimidine (FapyGua)
86 (Gassman et al. 2015). Surprisingly, despite the fact that both BPA and KBrO_3 induce oxidative
87 stress, an improvement in cellular survival was observed after co-exposure to both agents (Fig.
88 1).

89
90 Examination of this cellular protective effect revealed that in the early repair window of 4 h post
91 exposure, BPA co-exposure reduced DNA strand break signaling and resulted in the persistence
92 of oxidatively induced DNA lesions (Table 1) (Gassman et al. 2015), beyond the typical DNA
93 repair window of 2-4 h (Hollenbach et al. 1999; Jaruga and Dizdaroglu 1996). Given that
94 induction of oxidative stress can have profound consequences on the cellular microenvironment
95 and that the sustained oxidative insult has been shown to play a role in pathological processes,
96 such as inflammation, cancer, and neurodegenerative diseases (Benhar et al. 2002; Roberts et al.
97 2009), understanding how BPA co-exposure is improving cell survival and evading cell death is
98 critical to understanding the consequences of ubiquitous exposure to BPA.

99
100 In this work, we examined cellular microenvironment changes induced by BPA exposure at 4
101 and 24 h. Whole-genome microarray analysis was performed to evaluate the global

102 transcriptome changes associated with co-exposure of BPA and KBrO₃ at these two time points
103 and to identify gene targets induced by co-exposure that promote cell survival. Further,
104 microenvironment changes in chromatin structure, glutathione content, and pH induced by
105 exposure to BPA, KBrO₃, or both agents at these time points were also examined, to characterize
106 the adaptive response induced by co-exposure.

107

108 **Material and Methods**

109 **Chemicals.** BPA (Sigma Aldrich, St. Louis, MO) was prepared in absolute ethanol and diluted to
110 the final working concentration in medium. KBrO₃ was dissolved directly in the medium at the
111 time of the experiment.

112

113 **Cell culture.** Ku70^{-/-} mouse embryonic fibroblasts (MEFs) (a gift from Dr. Shigemi Matsuyama,
114 Cleveland, OH) were grown at 37 °C in a 10 % CO₂ incubator in Dulbecco's modified Eagle's
115 medium (DMEM) supplemented with glutamine, 10 % fetal bovine serum (FBS; HyClone,
116 Logan, UT), 1 % non-essential amino acids, and 1 % sodium pyruvate (Gama et al. 2009). Cells
117 were routinely tested and found to be free of mycoplasma contamination.

118

119 **RNA isolation.** Ku70^{-/-} cells were seeded in 145 mm dishes at 1×10^6 cells/dish and cultured to 80
120 % confluency. Cells were then treated with BPA, KBrO₃ or co-exposed to BPA and KBrO₃.
121 KBrO₃ only cells were treated for 1 h with 20 mM KBrO₃, washed with Hanks' balanced salt
122 solution (HBSS, Hyclone), then fresh medium was added to cells. Cells were allowed to repair
123 for an additional 3 or 23 h following treatment. For BPA only treatment, cells were incubated for
124 4 or 24 h in medium containing 150 μM BPA. For co-exposure, cell were incubated with 150 μM

125 BPA for 1 h, then 20 mM KBrO₃ and 150 μM BPA for 1 h, washed with HBSS, then fresh
126 medium with 150 μM BPA was added, and cells were allowed to repair for an additional 3 or 23
127 h. 4 and 24 h after treatment, cells were washed twice in phosphate buffered saline (PBS,
128 Hyclone), and total cellular RNA was isolated using the RNeasy Midi Kit (Qiagen, Valencia,
129 CA) according to the manufacturer's instructions. Residual genomic DNA was removed by on-
130 column digestion with RNase-free DNase I (Qiagen). Denaturing formaldehyde/agarose gel
131 electrophoresis validated quality and integrity of RNA samples, and the samples were quantified
132 by a Nanodrop ND-1000 spectrophotometer (Thermo Scientific, Wilmington, DE), and purity
133 was analyzed by the 260:280 absorbance ratio. Three biological replicates were collected and
134 isolated for the control and for all the treatment conditions.

135

136 ***Microarray study.*** Gene expression analysis was performed using Agilent Whole Mouse
137 Genome 4 × 44 multiplex format oligo arrays (Agilent Technologies, Santa Clara, CA) following
138 the Agilent one-color microarray-based gene expression analysis protocol. Starting with 500 ng
139 of total RNA, Cy3 labeled cRNA was produced according to manufacturer's protocol. For each
140 sample, 1.65 μg of Cy3 labeled cRNA was fragmented and hybridized for 17 hours in a rotating
141 hybridization oven. Slides were washed and then scanned with an Agilent Scanner. Data were
142 obtained using the Agilent Feature Extraction software (v9.5), using the 1-color defaults for all
143 parameters. The Agilent Feature Extraction Software performed error modeling, adjusting for
144 additive and multiplicative noise. The resulting data were processed using Omicsoft Array
145 Studio (Version 7.0) software. Significant probes were determined by filtering data to include
146 only probes with fold changes greater than 1.5 or less than -1.5 over control and *p* values < 0.01,
147 determined by an error-weighted one-way analysis of variance (ANOVA) and Bonferroni

148 multiple test correction using the Omicsoft software. This list of differentially expressed genes
149 generated by the Omicsoft software was used as an input for the curated pathway database,
150 Ingenuity Pathway Analysis (IPA; Ingenuity® Systems, Redwood City, CA;
151 www.ingenuity.com). IPA's Core analysis module used the differentially expressed gene list to
152 enrich for canonical and functional pathways or regulatory connections and to remove duplicates
153 and unmapped genes. Significance values were calculated using a right-tailed Fisher's exact test
154 to determine if a pathway was overrepresented by calculating whether genes in a specific
155 pathway were enriched within the data set compared to all genes on the array in the same
156 pathway at a $p < 0.05$ cutoff for significance based on IPA threshold recommendations. Only
157 pathways with a p value exceeding threshold and having more than two representative genes in
158 the data set were considered. Final filtered gene lists generated by IPA were input into Partek®
159 Genomic Suite software to create heat maps of hierarchical clustered genes and into
160 <http://www.pangloss.com/seidel/Protocols/venn.cgi> to create Venn diagrams.

161

162 ***Chromatin condensation.*** The level of chromatin condensation was measured with the
163 Chromatin Condensation & Membrane Permeability Dead Cell Apoptosis Kit (Life
164 Technologies, Carlsbad, CA) similar to (Muders et al. 2009). Ku70^{-/-} cells were seeded in 100
165 mm dishes at 1×10^6 cells/dish, then treated on the following day with BPA, KBrO₃ or co-
166 exposed, as described above. 4 or 24 h after the initiation of treatment, cells were harvested using
167 0.25 % trypsin, washed in 5 ml of PBS, and stained in 1 ml of PBS with 1 μ L each of Hoechst
168 33342 stock solution, YO-PRO-1 stock solution, and propidium iodide (PI) stock solution at
169 room temp for 15 min. Staurosporine treated cells were analyzed as a control for condensed
170 chromatin. Cells were incubated with 2 μ M staurosporine for 4 h at 37 °C, then harvested and

171 stained as described for BPA, KBrO₃ or co-exposed samples. Stained cells were analyzed with
172 Becton Dickinson LSRII flow cytometer (BD, Franklin Lakes, NJ, USA). Cells are separated
173 using the Hoechst and PI channels, and the mean fluorescent intensity was recorded for the
174 Hoechst channel. Mean intensities \pm standard error of mean (SEM) for at least three experiments
175 are reported.

176 ***Reduce glutathione assay.*** Levels of cellular reduced glutathione (GSH) were analyzed using
177 ThiolTracker Violet GSH detection reagent® (Life Technologies) according to the
178 manufacturer's protocol. Ku70^{-/-} cells were seeded in 100 mm dishes at 1×10^6 cells/dish, and
179 treated, as described above. 4 or 24 h after the initiation of treatment, cells were harvested using
180 0.25 % trypsin, washed in 4 ml of PBS, then stained in PBS containing 10 μ M ThiolTracker
181 Violet for 30 min at 37 °C. Stained cells were analyzed by flow cytometry on the LSRII, and
182 the mean fluorescent intensity was recorded for ThiolTracker Violet. Mean intensities \pm SEM of
183 three experiments are reported.

184
185 ***pH measurement.*** Intracellular pH was quantified by flow cytometry with the pHrodo® Red AM
186 Intracellular pH Indicator (Life Technologies) using the manufacturer's protocol. pHrodo is
187 weakly fluorescent at neutral pH and increasingly fluorescent in acidic pH, with a detectable pH
188 range reported from 4 to 9. Ku70^{-/-} cells were seeded in 100 mm dishes at 1×10^6 cells/dish, and
189 then treated, as described above, with BPA, KBrO₃, or co-exposed to both agents. Additionally,
190 for every experiment a calibration curve was prepared using the Intracellular pH Calibration
191 Buffer Kit (Life Technologies). 4 or 24 h after the initiation of treatment, cells were harvested
192 using 0.25 % trypsin, washed in 4 ml of PBS, and stained with pHrodo® Red at 37 °C for 30
193 min. Cells were then washed twice in PBS, and the calibration curve samples were resuspended

194 in valinomycin and nigericin with the pH calibration buffers of pH 5.5, 6.5, and 7.5 for 5 min
195 prior to analysis, per the manufacturer's protocol. The addition of valinomycin and nigericin
196 assists in the equilibration of the intracellular space with the pH buffer. Samples were then
197 analyzed by flow cytometry on the LSRII, and the mean fluorescent intensity was recorded for
198 pHRodo Red. A standard curve was prepared using the calibration buffer intensities, and the pH
199 for the control and treated samples were calculated. Mean pH values \pm SEM calculated for four
200 experiments are reported.

201

202 ***Measurement of oxidatively induced DNA lesions.*** Gas chromatography/tandem mass
203 spectrometry (GC-MS/MS) with isotope-dilution was used to identify and quantify modified
204 DNA bases in DNA as described previously (Gassman et al. 2015).

205

206 ***Statistical Analysis.*** Measured DNA lesions are expressed as mean \pm standard deviation (SD),
207 and all values are expressed as mean \pm standard error of mean (SEM). The data were analyzed by
208 means of ANOVA and Turkey post hoc analysis. $p < 0.05$ denoted by * were considered to
209 correspond with statistical significance.

210

211 **Results**

212 ***BPA alters mRNA expression of DNA repair genes***

213 To examine cellular changes induced by BPA, KBrO₃, and the co-exposure conditions, we
214 performed whole genome microarray analysis of untreated and treated cells 4 and 24 h after
215 treatment. Gene lists were generated from the average of three biological replicates for each
216 condition and significant probes were identified by selecting those probes showing p value $<$

217 0.01, determined by error-weighted ANOVA with Bonferroni multiple test correction. Duplicate
218 reads and non-coding genes were removed by IPA software. At 4 h post-damage induction,
219 7360 genes were altered after treatment with KBrO_3 , BPA or co-exposure, while 5126 significant
220 gene changes were observed 24 h after damage induction. Figure 2A shows a heat map of the
221 observed gene expression changes 4 h after treatment, while Figure 3A shows the observed
222 changes at 24 h. Figure 2B shows a Venn diagram analysis of the gene list 4 h post-damage
223 induction and illustrates the common and unique gene expression changes among the treatment
224 groups. Figure 3B shows the Venn diagram of these changes at 24 h post-damage induction.

225
226 The early response gene changes observed at 4 h show significant commonalities between
227 KBrO_3 only and BPA + KBrO_3 treatments (2008 genes), and an overlap of 569 genes between all
228 treatment groups is shown. IPA was used to identify the networks significantly regulated in
229 response to each treatment, and Tables 2 and 3 show the top ranked networks for each treatment
230 condition and the top induced and repressed genes, respectively. Despite the overlap observed,
231 there were only limited commonalities in the networks identified for each of the treatments
232 groups at 4 h (e.g., cellular development). Tables 4 and 5 show the top ranked networks and
233 induced and repressed genes observed after 24 h, and again limited commonalties are observed
234 between treatment groups (e.g., cancer, embryonic development, cellular movement). Overall,
235 each treatment condition altered network signaling and gene expression in a different manner,
236 with the most overlap observed for the KBrO_3 and co-exposure conditions, as illustrated by the
237 heat maps and Venn diagrams (Figs. 2 and 3).

238

239 Each of the treatments also generated a number of unique gene changes, and the co-exposure
240 condition generated 755 significant gene changes at each time point. Of these gene expression
241 changes, only 86 genes were common between the two time points (Fig. 4). IPA was performed
242 on these unique gene sets, and the top 5 networks significantly regulated by co-exposure at 4 and
243 24 h are shown in Table 6.

244
245 The 24 h pathway analysis showed a significant up-regulation of DNA repair genes that address
246 oxidatively induced DNA damage, indicating that the BPA co-exposure induced an adaptive
247 response after the 4 h time point; this is consistent with our previous results showing a repression
248 of DNA repair at the 4 h time point (Gassman et al. 2015). Figure 5A and B shows the two DNA
249 Replication, Recombination networks altered by the co-exposure condition. Gene expression
250 changes for DNA repair proteins of particular interest to oxidative repair that are unique to the
251 co-exposure condition are also shown in Table 7.

252

253 ***BPA alters chromatin condensation to improve cell survival***

254 The adaptive response induced by BPA co-exposure does not occur within the first 4 h of
255 exposure, where repair of oxidatively induced DNA lesions typically occurs (Hollenbach et al.
256 1999; Jaruga and Dizdaroglu 1996). If DNA repair of the induced DNA lesions occurred
257 normally during the first 4 h post exposure, toxic DNA strand break intermediates would be
258 generated, and these intermediates could induce cell death, as observed for the KBrO_3 only
259 treatment shown in Figure 1. The improved survival observed after co-exposure indicated that
260 DNA repair was being suppressed, and our previous work demonstrated that BPA co-exposure
261 suppressed the removal of oxidatively induced DNA lesions from genomic DNA within 4 h of

262 the damage induction (Table 1) (Gassman et al. 2015). This lesion persistence indicated a lesion
263 excision defect, yet BPA exposure and KBrO_3 exposure generated a number of oxidatively
264 induced DNA lesions (5'-hydroxycytosine, thymine glycol (ThyGly), FapyGua, and 8-oxo-
265 guanine (8-oxoGua)) that are addressed by several different DNA glycosylases (Nei1, Nth1, and
266 Ogg1) (Gassman et al. 2015). However, chromatin structure regulates the access of DNA repair
267 proteins to sites of DNA damage, and alterations in the chromatin structure has been shown to
268 reduce excision of lesions, like 8-oxoGua (Amouroux et al. 2010). This structural change could
269 create a lesion excision defect for a number of DNA glycosylases.

270

271 To evaluate chromatin structure after BPA exposure and co-exposure, we utilized a flow
272 cytometry assay to measure the degree of compaction utilizing a DNA intercalating dye, Hoechst
273 33342. Hoechst 33342 brightly stains the condensed chromatin of apoptotic cells and dimly
274 stains the normal chromatin of live cells (Belloc et al. 1994). Using the flow cytometry assay, the
275 shift in the mean intensity of the Hoechst dye can reveal the degree of chromatin compaction
276 induced by treatment (Fig. 6). With this technique, compaction of chromatin was observed 4 h
277 after treatment with BPA alone and co-exposure with BPA with KBrO_3 ($156 \% \pm 12.5 \%$ and
278 $128 \% \pm 14.4 \%$ of control, respectively). This compaction may prevent DNA glycosylases from
279 accessing oxidatively induced DNA lesions and is consistent with the lesion persistence and
280 strand break signaling reduction previously reported (Gassman et al. 2015).

281

282 At 24 h, the degree of chromatin compaction for BPA treated cells was reduced significantly
283 from the 4 h time point, but was still slightly higher than untreated cells ($110 \% \pm 2.7 \%$ of
284 control). On the other hand, the KBrO_3 treated cells now showed compaction ($133 \pm 5.3 \%$ of

285 control), indicating that KBrO₃ treated cells may be beginning to undergo apoptosis. Finally, co-
286 exposed cells were consistent with untreated cells (99.6 ± 6.5 %).

287

288 These differences in levels of chromatin compaction are consistent with and supported by the
289 microarray analysis: at 4 h post-damage induction, the results show a reduction in DNA repair
290 gene expression for both KBrO₃ only and BPA co-exposure conditions. Table 8 shows the gene
291 expression changes for genes involved in oxidative damage repair. Overall, a significant
292 reduction in gene expression was observed for glycosylases involved in lesion removal for both
293 KBrO₃ and co-exposure conditions.

294

295 ***BPA co-exposure promotes lesion removal after 4 h***

296 Previously, we determined that a significant amount of oxidatively induced DNA lesions
297 persisted in the genomic DNA 4 h after DNA damage induction (Table 1 and (Gassman et al.
298 2015)), and this is consistent with the observed compaction of cellular chromatin. Since this
299 compaction was reduced 24 h after co-exposure, and the microarray analysis supports the up-
300 regulation of DNA repair genes, we quantified oxidatively induced DNA lesions in DNA
301 isolated from treated cells 24 h after damage induction; the aim was to determine if these lesions
302 were repaired or instead persisted in the genomic DNA. GC-MS/MS with isotope-dilution, as
303 described (Reddy et al. 2013) (Gassman et al. 2015), was used to quantify lesions in isolated
304 nuclear DNA. The mean values for the quantified DNA lesions are summarized in Table 9.

305

306 Our previous results showed a significant accumulation of lesions for BPA only (ThyGly) and
307 for BPA and KBrO₃ co-exposure (ThyGly, FapyAde, and FapyGua) 4 h after damage induction

308 (Table 1 and (Gassman et al. 2015)). Here, we observed no significant accumulation of lesions
309 24 h after damage induction. The ThyGly and FapyAde levels were consistent with or lower than
310 control; the FapyGua levels reflect a slight, but non-significant, increase in lesion content over
311 control; and 8-oxoGua shows a slight, but non-significant, decrease in lesion content. These
312 results demonstrate that despite the initial persistence of lesions 4 h after exposure, the induced
313 adaptive response promoted repair of these lesions between 4 and 24 h.

314

315 *BPA exposure alters GSH levels over time*

316 In addition to generating oxidatively induced DNA lesions, exposure to oxidative stress can alter
317 the cellular microenvironment and reduce the cellular redox balance. Depletion of intracellular
318 glutathione has been previously observed after BPA exposure (Jain et al. 2011; Kabuto et al.
319 2003; Wu et al. 2013). To confirm that BPA alter the cellular microenvironment in a time-
320 dependent manner, we measured depletion of intracellular GSH with a fluorescent dye,
321 ThiolTracker Violet, which reacts with reduced thiols in live cells. At 4 h after exposure, the
322 GSH levels in the treated cells were consistent with control, though a small shoulder in the mean
323 intensity profile of the ThiolTracker dye appeared in both BPA samples; this indicates that GSH
324 was beginning to be depleted (Fig. 7). At 24 h after exposure, the GSH levels of cells exposed to
325 BPA were slightly reduced, and a clear second population was observed in the co-exposed cells
326 (Fig. 7).

327

328 *BPA preserves intracellular pH after oxidative stress*

329 Induction of oxidative stress and depletion of intracellular GSH can also induce changes in
330 intracellular pH. To determine the effect BPA exposure has on intracellular pH, we measured

331 intracellular pH at 4 and 24 h after treatment (Table 10). At 4 h post-damage induction, KBrO_3
332 alone induced a shift in intracellular pH to 6.8. Treatment with BPA alone had no effect, and the
333 co-exposure condition showed a reduction in pH. However, BPA co-exposure significantly
334 reduced the acidification caused by the KBrO_3 treatment ($p < 0.01$). At 24 h post-damage
335 induction, the pH with KBrO_3 alone was more basic compared to control, while the co-exposure
336 condition is now significantly acidic compared to control. The delay in pH drop may be due to
337 the depletion of GSH, as observed in Figure 7. Overall, the BPA co-exposure mitigated the pH
338 alterations induced by KBrO_3 -induced oxidative stress.

339

340 **Discussion**

341 Numerous reports have indicated that BPA exposure induces global transcriptome and epigenetic
342 changes that can have long-term consequences for cellular regulatory networks and signal
343 transduction pathways (Bromer et al. 2010; Fernandez et al. 2012; Lee et al. 2008; Naciff et al.
344 2002; Patterson et al. 2015; Ptak et al. 2011; Tabuchi et al. 2006; Weng et al. 2010; Yin et al.
345 2014). While dosing conditions and exposure times can be highly variable in the literature, most
346 studies report alterations in DNA response and repair pathways, and a number of studies have
347 demonstrated BPA exposure induces oxidative stress and oxidatively induced DNA lesions
348 (Babu et al. 2013; Gassman et al. 2015; Jain et al. 2011; Kabuto et al. 2003; Lee et al. 2008;
349 Tiwari et al. 2012; Wu et al. 2013; Yang et al. 2009). However, features of how the cellular
350 microenvironment reacts to the BPA-induced oxidative stress and responds to the induced DNA
351 damage have been less well understood. Here, we present evidence that BPA exposure alters the
352 microcellular environment to promote cell survival after the induction of additional oxidative
353 stress by the oxidizing agent, KBrO_3 .

354

355 Our previous work established the pro-survival effects of BPA and KBrO_3 co-exposure and
356 identified a persistence of oxidatively induced DNA lesions 4 h after damage induction (Table 1
357 and (Gassman et al. 2015)). Here, we demonstrate that this persistence is caused by the
358 compaction of chromatin in the presence of BPA (Fig. 6). This type of compaction has been
359 previously reported after oxidative stress induced by hydrogen peroxide (O'Hagan et al. 2011),
360 KBrO_3 (Amouroux et al. 2010), and light activation of the KillerRed fluorescent protein (Lan et
361 al. 2014), but the time scale for the compaction appears to be extended in the presence of BPA.
362 Compaction of chromatin regions containing oxidatively induced DNA lesions have been shown
363 to reduce recruitment of the DNA glycosylase Ogg1, delaying the repair of oxidatively induced
364 DNA lesions (Amouroux et al. 2010). This remodeling of chromatin is also reflected in the
365 down-regulation of DNA repair proteins involved in BER observed in the microarray analysis
366 (Table 8).

367

368 Coupled with the observed chromatin changes 4 h post-damage initiation, BPA co-exposure also
369 significantly stabilizes the drop in intracellular pH induced by KBrO_3 (Table 10). Oxidative
370 stress alters the balance intracellular redox machinery and can modify cellular membrane ion
371 transport channels (Clerici et al. 1992). Changes in the cellular Na^+/H^+ antiporter activity and an
372 increase in intracellular pH have been reported after exposure of estrogen and estradiol (Ediger et
373 al. 1999; Incerpi et al. 2003; Kilic et al. 2009). Here, no increase in intracellular pH is observed
374 after BPA exposure, and to our knowledge, no reports of intracellular pH changes with BPA
375 exposure have been previously reported.

376

377 While depletion of GSH by ROS often results in changes in the cellular Na^+/H^+ antiporter
378 activity and is associated with drop in intracellular pH (Ciriolo et al. 1997; Cutaia and Parks
379 1994), our conditions show no significant depletion of GSH at 4 h post-damage induction for any
380 of our treatment conditions (Fig. 7). The intracellular pH drop observed after KBrO_3 treatment is
381 most likely a results of the increase in free K^+ released upon the formation of the reactive
382 bromate anions. Effects of K^+ efflux from KCl exposure have been previously described in the
383 literature (Adler and Fraley 1977), though our observation of a decrease in intracellular pH
384 following KBrO_3 exposure is the first to our knowledge. There are numerous possible
385 explanations for how BPA exposure prevents the drop in intracellular pH, from activation of the
386 mitogen-activated protein kinases (MAPK) pathway (Lee et al. 2008) to stimulation of the
387 antiporter system. Further studies are needed to explore the mechanism by which BPA stabilizes
388 against the drop in intracellular pH.

389

390 At 24 h post-damage induction, the suppressive aspects of BPA exposure observed at the 4 h
391 time point have now transitioned into cellular microenvironment changes conducive to DNA
392 repair. An adaptive response is stimulated in the time period between 4 and 24 h that results in
393 chromatin relaxation. Chromatin structure compaction, compared to control at 4 h, is now
394 consistent with the control untreated cells, while KBrO_3 treated cells now show compact
395 chromatin consistent with progression into apoptosis (Fig. 6). The relaxation of chromatin is also
396 reflected in the microarray results where up-regulation of DNA repair genes involved in the
397 repair of oxidatively induced DNA damage is observed (Table 7). Repair of oxidatively induced
398 DNA lesions, which was suppressed 4 h after damage induction (Gassman et al. 2015), is
399 observed in the GC-MS/MS quantification of lesion (Table 9). All measured lesions in treated

400 cells were consistent with the lesion levels measured in untreated controls, reflecting the excision
401 and repair of the oxidatively induced DNA lesions measured at 4 h by the DNA repair
402 machinery.

403
404 Finally, 24 h post-damage initiation a reduction in GSH is observed in BPA exposed cells, and
405 the intracellular pH of the co-exposed cells has dropped significantly compared to control;
406 however, unlike the KBrO₃ only cells, the pH is still within physiological pH values. GSH
407 depletion has been previously observed after exposure to BPA and has been hypothesized to
408 contribute to its pro-oxidant effects (Babu et al. 2013).

409
410 Together these results support a dynamic alteration of the cellular microenvironment that is
411 initiated after co-exposure in our mouse fibroblast model system (Fig. 8). While BPA exposure
412 alone can alter gene expression (Bromer et al. 2010; Fernandez et al. 2012; Lee et al. 2008;
413 Naciff et al. 2002; Patterson et al. 2015; Ptak et al. 2011; Tabuchi et al. 2006; Weng et al. 2010;
414 Yin et al. 2014), deplete GSH (Jain et al. 2011; Kabuto et al. 2003; Wu et al. 2013), and induce
415 oxidative stress in cells (Babu et al. 2013; Jain et al. 2011; Nishimura et al. 2014a; Xin et al.
416 2014; Yang et al. 2009), this work demonstrates that BPA exposure coupled with endogenous or
417 exogenous stresses, like KBrO₃-induced oxidative stress, can dramatically alter the microcellular
418 environment and can delay and alter DNA damage response and repair. These effects are largely
419 uncharacterized in the literature, where focus has been on examining the endocrine disrupting
420 functions of BPA or characterization of DNA damage effects of BPA exposure alone. The
421 ubiquitous nature of BPA and its analogs coupled with its pro-oxidant activities and the adaptive
422 response, identified here, indicate that BPA co-exposure may influence disease development and

423 progression, particularly inflammatory diseases, which have been linked to BPA exposure
424 (Bindhumol et al. 2003; Chitra et al. 2003; Yang et al. 2009).

425

426 **Conclusions**

427 Co-exposure of BPA with the oxidizing agent KBrO_3 alters the cellular microenvironment and
428 induces an adaptive response that promotes cell survival, despite an increase in oxidative stress.
429 BPA exposed cells undergo an initial period of DNA repair suppression following exogenous
430 damage induction by KBrO_3 , which is followed by an induced adaptive response, unique to the
431 co-exposure condition, resulting in whole genome expression changes, chromatin remodeling,
432 depletion of intracellular GSH, and alterations in intracellular pH. Further studies are required to
433 better characterize the long-term consequences of this induced adaptive response, since co-
434 exposure of BPA with endogenous and exogenous agents mimics the environmental exposures to
435 which the population is exposed.

436

437 **References**

- 438 Adler S, Fraley DS. 1977. Potassium and intracellular pH. *Kidney Int* 11:433-442.
- 439 Amouroux R, Campalans A, Epe B, Radicella JP. 2010. Oxidative stress triggers the preferential
440 assembly of base excision repair complexes on open chromatin regions. *Nucleic Acids Res*
441 38:2878-2890.
- 442 Babu S, Uppu S, Claville MO, Uppu RM. 2013. Prooxidant actions of bisphenol A (BPA)
443 phenoxyl radicals: Implications to BPA-related oxidative stress and toxicity. *Toxicology Mech*
444 *Methods* 23:273-280.
- 445 Belloc F, Dumain P, Boisseau MR, Jalloustre C, Reiffers J, Bernard P, et al. 1994. A flow
446 cytometric method using hoechst 33342 and propidium iodide for simultaneous cell cycle
447 analysis and apoptosis determination in unfixed cells. *Cytometry* 17:59-65.
- 448 Benhar M, Engelberg D, Levitzki A. 2002. ROS, stress-activated kinases and stress signaling in
449 cancer. *EMBO Rep* 3:420-425.
- 450 Bindhumol V, Chitra KC, Mathur PP. 2003. Bisphenol A induces reactive oxygen species
451 generation in the liver of male rats. *Toxicology* 188:117-124.
- 452 Bromer JG, Zhou Y, Taylor MB, Doherty L, Taylor HS. 2010. Bisphenol-A exposure in utero
453 leads to epigenetic alterations in the developmental programming of uterine estrogen response.
454 *FASEB J* 24:2273-2280.
- 455 Chitra KC, Latchoumycandane C, Mathur PP. 2003. Induction of oxidative stress by bisphenol A
456 in the epididymal sperm of rats. *Toxicology* 185:119-127.
- 457 Choi YJ, Li H, Son MY, Wang XH, Fornsgaglio JL, Sobol RW, et al. 2014. Deletion of individual
458 Ku subunits in mice causes an nhej-independent phenotype potentially by altering
459 apurinic/aprimidinic site repair. *PLoS One* 9:e86358.
- 460 Ciriolo MR, Palamara AT, Incerpi S, Lafavia E, Bue MC, De Vito P, et al. 1997. Loss of GSH,
461 oxidative stress, and decrease of intracellular pH as sequential steps in viral infection. *J Biol*
462 *Chem* 272:2700-2708.

- 463 Clerici C, Friedlander G, Amiel C. 1992. Impairment of sodium-coupled uptakes by hydrogen
464 peroxide in alveolar type II cells: protective effect of D-alpha-tocopherol. *Am J Physiol*
465 262:L542-548.
- 466 Cutaia M, Parks N. 1994. Oxidant stress decreases Na⁺/H⁺ antiport activity in bovine pulmonary
467 artery endothelial cells. *Am J Physiol* 267:L649-659.
- 468 Ediger TR, Kraus WL, Weinman EJ, Katzenellenbogen BS. 1999. Estrogen receptor regulation
469 of the Na⁺/H⁺ exchange regulatory factor. *Endocrinology* 140:2976-2982.
- 470 Fernandez SV, Huang Y, Snider KE, Zhou Y, Pogash TJ, Russo J. 2012. Expression and DNA
471 methylation changes in human breast epithelial cells after bisphenol A exposure. *Int J Oncol*
472 41:369-377.
- 473 Gama V, Gomez JA, Mayo LD, Jackson MW, Danielpour D, Song K, et al. 2009. Hdm2 is a
474 ubiquitin ligase of Ku70-Akt promotes cell survival by inhibiting Hdm2-dependent Ku70
475 destabilization. *Cell Death Differ* 16:758-769.
- 476 Gassman NR, Coskun E, Stefanick DF, Horton JK, Jaruga P, Dizdaroglu M, et al. 2015.
477 Bisphenol A promotes cell survival following oxidative DNA damage in mouse fibroblasts.
478 *PLoS One* 10:e0118819.
- 479 Hollenbach S, Dhenaut A, Eckert I, Radicella JP, Epe B. 1999. Overexpression of OGG1 in
480 mammalian cells: Effects on induced and spontaneous oxidative DNA damage and mutagenesis.
481 *Carcinogenesis* 20:1863-1868.
- 482 Incerpi S, D'Arezzo S, Marino M, Musanti R, Pallottini V, Pascolini A, et al. 2003. Short-term
483 activation by low 17beta-estradiol concentrations of the Na⁺/H⁺ exchanger in rat aortic smooth
484 muscle cells: Physiopathological implications. *Endocrinology* 144:4315-4324.
- 485 Iso T, Watanabe T, Iwamoto T, Shimamoto A, Furuichi Y. 2006. DNA damage caused by
486 bisphenol A and estradiol through estrogenic activity. *Biol Pharm Bull* 29:206-210.
- 487 Jain S, Kumar CH, Suranagi UD, Mediratta PK. 2011. Protective effect of N-acetylcysteine on
488 bisphenol A-induced cognitive dysfunction and oxidative stress in rats. *Food Chemical Toxicol*
489 49:1404-1409.
- 490 Jaruga P, Dizdaroglu M. 1996. Repair of products of oxidative DNA base damage in human
491 cells. *Nucleic Acids Res* 24:1389-1394.

- 492 Kabuto H, Hasuike S, Minagawa N, Shishibori T. 2003. Effects of bisphenol A on the
493 metabolisms of active oxygen species in mouse tissues. *Environ Res* 93:31-35.
- 494 Kilic A, Javadov S, Karmazyn M. 2009. Estrogen exerts concentration-dependent pro-and anti-
495 hypertrophic effects on adult cultured ventricular myocytes. Role of NHE-1 in estrogen-induced
496 hypertrophy. *J Mol Cell Cardiol* 46:360-369.
- 497 Lan L, Nakajima S, Wei L, Sun L, Hsieh CL, Sobol RW, et al. 2014. Novel method for site-
498 specific induction of oxidative DNA damage reveals differences in recruitment of repair proteins
499 to heterochromatin and euchromatin. *Nucleic Acids Res* 42:2330-2345.
- 500 Lee S, Suk K, Kim IK, Jang IS, Park JW, Johnson VJ, et al. 2008. Signaling pathways of
501 bisphenol A-induced apoptosis in hippocampal neuronal cells: Role of calcium-induced reactive
502 oxygen species, mitogen-activated protein kinases, and nuclear factor-kappa beta. *J Neurosci Res*
503 86:2932-2942.
- 504 Li H, Marple T, Hasty P. 2013. Ku80-deleted cells are defective at base excision repair. *Mutat*
505 *Res* 745-746:16-25.
- 506 Muders MH, Zhang H, Wang E, Tindall DJ, Datta K. 2009. Vascular endothelial growth factor-c
507 protects prostate cancer cells from oxidative stress by the activation of mammalian target of
508 rapamycin complex-2 and Akt-1. *Cancer Res* 69:6042-6048.
- 509 Naciff JM, Jump ML, Torontali SM, Carr GJ, Tiesman JP, Overmann GJ, et al. 2002. Gene
510 expression profile induced by 17alpha-ethynyl estradiol, bisphenol A, and genistein in the
511 developing female reproductive system of the rat. *Toxicol Sci* 68:184-199.
- 512 Nishimura Y, Nagao T, Fukushima N. 2014. Long-term pre-exposure of pheochromocytoma
513 pc12 cells to endocrine-disrupting chemicals influences neuronal differentiation. *Neurosci Lett*
514 570:1-4.
- 515 O'Hagan HM, Wang W, Sen S, Destefano Shields C, Lee SS, Zhang YW, et al. 2011. Oxidative
516 damage targets complexes containing DNA methyltransferases, sirt1, and polycomb members to
517 promoter cpG islands. *Cancer Cell* 20:606-619.
- 518 Patterson AR, Mo X, Shapiro A, Wernke KE, Archer TK, Burd CJ. 2015. Sustained
519 reprogramming of the estrogen response after chronic exposure to endocrine disruptors. *Mol*
520 *Endocrinol* 29:384-395.

- 521 Ptak A, Wróbel A, Gregoraszczyk EL. 2011. Effect of bisphenol-A on the expression of selected
522 genes involved in cell cycle and apoptosis in the OVCAR-3 cell line. *Toxicol Lett* 202:30-35.
- 523 Reddy PT, Jaruga P, Kirkali G, Tuna G, Nelson BC, Dizdaroglu M. 2013. Identification and
524 quantification of human DNA repair protein NEIL1 by liquid chromatography/isotope-dilution
525 tandem mass spectrometry. *J Proteome Res* 12:1049-1061.
- 526 Roberts RA, Laskin DL, Smith CV, Robertson FM, Allen EM, Doorn JA, et al. 2009. Nitritative
527 and oxidative stress in toxicology and disease. *Toxicol Sci* 112:4-16.
- 528 Tabuchi Y, Takasaki I, Kondo T. 2006. Identification of genetic networks involved in the cell
529 injury accompanying endoplasmic reticulum stress induced by bisphenol a in testicular sertoli
530 cells. *Biochem Biophys Res Commun* 345:1044-1050.
- 531 Tiwari D, Kamble J, Chilgunde S, Patil P, Maru G, Kawle D, et al. 2012. Clastogenic and
532 mutagenic effects of bisphenol a: An endocrine disruptor. *Mutat Res* 743:83-90.
- 533 Vandenberg LN, Hauser R, Marcus M, Olea N, Welshons WV. 2007. Human exposure to
534 bisphenol A (BPA). *Reprod Toxicol* 24:139-177.
- 535 Vandenberg LN, Chahoud I, Heindel JJ, Padmanabhan V, Paumgartten FJ, Schoenfelder G.
536 2010. Urinary, circulating, and tissue biomonitoring studies indicate widespread exposure to
537 bisphenol A. *Environ Health Perspect* 118:1055-1070.
- 538 Weng YI, Hsu PY, Liyanarachchi S, Liu J, Deatherage DE, Huang YW, et al. 2010. Epigenetic
539 influences of low-dose bisphenol A in primary human breast epithelial cells. *Toxicol Appl
540 Pharmacol* 248:111-121.
- 541 Wu HJ, Liu C, Duan WX, Xu SC, He MD, Chen CH, et al. 2013. Melatonin ameliorates
542 bisphenol A-induced DNA damage in the germ cells of adult male rats. *Mutat Res* 752:57-67.
- 543 Xin F, Jiang L, Liu X, Geng C, Wang W, Zhong L, et al. 2014. Bisphenol A induces oxidative
544 stress-associated DNA damage in INS-1 cells. *Mutat Res Genet Toxicol Environ Mutagen*
545 769:29-33.
- 546 Yang YJ, Hong YC, Oh SY, Park MS, Kim H, Leem JH, et al. 2009. Bisphenol A exposure is
547 associated with oxidative stress and inflammation in postmenopausal women. *Environ Res*
548 109:797-801.

549 Yin R, Gu L, Li M, Jiang C, Cao T, Zhang X. 2014. Gene expression profiling analysis of
550 bisphenol A-induced perturbation in biological processes in ER-negative HEK293 cells. PLoS
551 One 9:e98635.

552

553

554 **Table 1. Measured oxidatively damaged DNA bases in Ku70^{-/-} genomic DNA 4 h post-**
 555 **damage induction from (Gassman et al. 2015).**

	DNA lesion/ 10 ⁶ DNA bases (mean ± SD, n >3)			
	ThyGly	FapyAde	FapyGua	8-oxoGua
Control	3.82 ± 1.32	2.83 ± 0.98	3.69 ± 1.41	0.98 ± 0.16
BPA + KBrO ₃	7.48 ± 0.48*	4.38 ± 0.41*	6.77 ± 1.36*	1.55 ± 0.59

556 **p* < 0.05 compared with untreated controls

557

558 **Table 2. Top regulated networks 4 h post-damage induction****KBrO₃**

1. Cell Morphology, Cellular Assembly and Organization, Cellular Function and Maintenance
2. Cancer, Organismal Injury and Abnormalities, Reproductive System Disease
3. Hereditary Disorder, Neurological Disease, Lipid Metabolism
4. Cell-To-Cell Signaling and Interaction, Cellular Function and Maintenance, Hematological System Development and Function
5. Protein Synthesis, RNA Post-Transcriptional Modification, Carbohydrate Metabolism

BPA

1. Cellular Development, Cellular Growth and Proliferation, Organ Development
2. Cellular Movement, Immune Cell Trafficking, Connective Tissue Disorders
3. Cellular Development, Cellular Growth and Proliferation, Connective Tissue Development and Function
4. Neurological Disease, Cell-To-Cell Signaling and Interaction, Hematological System Development and Function
5. Dermatological Diseases and Conditions, Organismal Injury and Abnormalities, Lipid Metabolism

BPA + KBrO₃

1. Embryonic Development, Nervous System Development and Function, Organ Development
2. Cellular Growth and Proliferation, Infectious Disease, Protein Synthesis
3. Cell Cycle, Cellular Assembly and Organization, Reproductive System Development and Function
4. Developmental Disorder, Hereditary Disorder, Metabolic Disease
5. Organismal Development, Tissue Morphology, Drug Metabolism

559

560

561 **Table 3. Top induced and repressed genes 4 h post-damage induction**

KBrO ₃	Fold Change/Control	BPA	Fold Change/Control	BPA + KBrO ₃	Fold Change/Control
GSTA5	195.423	CCL20	60.37	IL18R1	150.272
IL18R1	165.986	CXCL3	55.581	GSTA5	118.712
AREG	131.227	Saa3	26.361	PTGS2	95.172
DUSP2	92.477	HCAR2	25.405	AREG	84.638
EGR4	65.351	EGR4	23.721	ATF3	81.49
KLF15	-56.007	LGALS12	-10.284	TNS1	-41.975
Cyp2d22	-35.115	DSC1	-8.749	Akr1b10	-39.628
IKZF2	-22.961	FRY	-5.689	FZD2	-35.905
BMF	-22.292	HPGD	-4.937	Cyp2d22	-35.268
Akr1b10	-21.197	PLCH2	-4.768	KAT2B	-30.719

562

563

564 **Table 4. Top regulated networks 24 h after damage induction****KBrO₃**

1. Cardiovascular System Development and Function, Cellular Movement, Cancer
2. Cell Death and Survival, Dermatological Diseases and Conditions, Developmental Disorder
3. Gastrointestinal Disease, Hepatic System Disease, Liver Cirrhosis
4. Cell Death and Survival, Drug Metabolism, Endocrine System Development and Function
5. Cancer, Organismal Injury and Abnormalities, Connective Tissue Disorders

BPA

1. Cellular Movement, Connective Tissue Development and Function, Organ Morphology
2. Connective Tissue Disorders, Organismal Injury and Abnormalities, Skeletal and Muscular Disorders
3. Cardiac Dysfunction, Cardiovascular Disease, Organismal Injury and Abnormalities
4. Organismal Development, Energy Production, Molecular Transport
5. Cell-To-Cell Signaling and Interaction, Cellular Movement, Hematological System Development and Function

BPA + KBrO₃

1. Dermatological Diseases and Conditions, Inflammatory Disease, Skeletal and Muscular Disorders
2. Amino Acid Metabolism, Small Molecule Biochemistry, Neurological Disease
3. Protein Synthesis, Cell Death and Survival, Embryonic Development
4. Cancer, Embryonic Development, Cellular Development
5. Cell Cycle, DNA Replication, Recombination, and Repair, Cancer

565

566

567 **Table 5. Top induced and repressed genes 24 h after damage induction**

KBrO ₃	Fold Change/Control	BPA	Fold Change/Control	BPA + KBrO ₃	Fold Change/Control
GSTA5	87.219	Wfdc17	37.229	GSTA5	181.836
ROBO3	22.114	Saa3	25.573	Prg4	62.482
Prg4	16.538	LCN2	19.522	ROBO3	59.949
BLNK	15.8	OSTN	16.42	MMP15	25.597
PTPN22	15.395	CA6	15.788	CA6	23.355
FGL2	-73.599	MYH1	-11.145	AGTR2	-153.275
CYP2F1	-59.905	Nbl	-10.875	HP	-125.757
SLCO2B1	-57.705	MYH2	-9.608	DIO3	-114.982
VIT	-55.675	SLC26A7	-9.425	SLCO2B1	-102.011
HP	-37.549	NPR3	-9.109	CYP2F1	-85.326

568

569

570 **Table 6. Top networks regulated by the unique co-exposure genes at 4 and 24 h after**
571 **damage induction**

4h

1. Nervous System Development and Function, Organ Morphology, Organismal Development
2. Energy Production, Nucleic Acid Metabolism, Small Molecule Biochemistry
3. Developmental Disorder, Hereditary Disorder, Metabolic Disease
4. RNA Post-Transcriptional Modification, Cancer, Hematological Disease
5. Connective Tissue Disorders, Skeletal and Muscular Disorders, Developmental Disorder

24 h

1. DNA Replication, Recombination, and Repair, Hereditary Disorder, Neurological Disease
 2. Cancer, Gastrointestinal Disease, Hepatic System Disease
 3. DNA Replication, Recombination, and Repair, Cellular Response to Therapeutics, Cell Cycle
 4. Gene Expression, Cancer, Hereditary Disorder
 5. Nucleic Acid Metabolism, Small Molecule Biochemistry, Amino Acid Metabolism
-

572

573

574 **Table 7. DNA repair genes associated with the co-exposure condition identified at 24 h**
 575 **post-damage induction**

Gene	Gene Name	Fold Change/Control
Ercc4	excision repair cross-complementation group 4, XPF	4.05
Ercc5	excision repair cross-complementation group 5, XPG	1.85
Ercc8	excision repair cross-complementation group 8, CSA	2.5
Ogg1	8-oxoguanine DNA glycosylase	1.86
Pol κ	polymerase (DNA directed) kappa	1.68
Rad50	RAD50 homolog (<i>S. cerevisiae</i>)	1.69
Rad51	RAD51 recombinase	2.35
Tdp1	tyrosyl-DNA phosphodiesterase 1	1.66
Xrcc5	X-ray repair complementing defective repair in Chinese hamster cells 5 (double-strand-break rejoining), Ku86	1.92

576

577

578 **Table 8. Gene expression changes observed for DNA repair genes 4 h after damage**
 579 **induction**

Gene	Gene Name	KBrO₃ Fold Change/Control	BPA + KBrO₃ Fold Change/Control
Ercc8	excision repair cross-complementation group 8, CSA	4.63	6.36
Mpg	N-methylpurine-DNA glycosylase	-1.91	-2.59
Nei1	nei endonuclease VIII-like 1 (E. coli)	-2.48	-2.46
Nei3	nei endonuclease VIII-like 3 (E. coli)	-6.24	-11.36
Ogg1	8-oxoguanine DNA glycosylase	-1.68	-2.00
Pol β	polymerase (DNA directed) beta	n.c.	-2.90
Pol λ	polymerase (DNA directed) lambda	-3.49	-2.92
Tdg	thymine-DNA glycosylase	2.12	2.82
Xrcc1	X-ray repair complementing defective repair in Chinese hamster cells 1	-1.72	-1.76

580 n.c. – no significant change over control

581

582 **Table 9. Levels of oxidatively induced DNA bases in Ku70^{-/-} genomic DNA 24 h after**
 583 **damage induction**

	DNA lesion/ 10 ⁶ DNA bases (mean ± SD, n >3)			
	ThyGly	FapyAde	FapyGua	8-oxoGua
Control	5.32 ± 0.80	3.61 ± 0.26	3.81 ± 0.83	3.25 ± 0.01
BPA	2.54 ± 0.69	2.75 ± 1.74	3.71 ± 1.88	3.09 ± 0.57
KBrO ₃	3.54 ± 0.27	3.21 ± 0.32	3.77 ± 1.31	2.84 ± 0.55
BPA + KBrO ₃	5.38 ± 1.74	3.35 ± 0.31	6.00 ± 2.02	2.80 ± 0.80

584

585 **Table 10. pH_{Rodo} determined intracellular pH (n ≥ 4)**

pH		
Control	7.5 ± 0.11	
	<u>4 h</u>	<u>24 h</u>
BPA	7.5 ± 0.28	7.5 ± 0.11
KBrO ₃	6.8 ± 0.11 *	7.8 ± 0.26
BPA + KBrO ₃	7.2 ± 0.08	7.0 ± 0.14 *

586 **p* < 0.05 compared with untreated controls.

587

588 Figure 1. Cell survival following co-exposure of BPA and KBrO_3 from (Gassman et al. 2015).
589 Ku70 -deficient cells were treated with increasing amounts of KBrO_3 for 1 h (solid circles) or
590 pre-treated with $150 \mu\text{M}$ BPA for 1 h, co-exposed with BPA and increasing amounts of KBrO_3
591 for 1 h, then BPA exposure was continued for a total of 24 h (open circles), as described in
592 (Gassman et al. 2015).

593

594 Figure 2. Gene expression changes observed by whole genome analysis of mRNA isolated 4 h
595 after treatment with KBrO_3 , BPA, or co-exposure of both agents, as described in Material and
596 Methods. (A) Heat map of gene expression changes observed after treatment was generated
597 using Partek® Genomic Suite software with probes selected by a fold-change cutoff of ± 1.5
598 compared to untreated controls and an ANOVA-calculated significance level of $p < 0.01$ ($n = 3$).
599 (B) Significant probe changes identified using the described criteria are sorted by Venn diagram.

600

601 Figure 3. Gene expression changes observed by whole genome analysis of mRNA isolated 24 h
602 after treatment with KBrO_3 , BPA, or co-exposure of both agents, as described in Material and
603 Methods. (A) Heat map of gene expression changes observed after treatment was generated
604 using Partek® Genomic Suite software with probes selected by a fold-change cutoff of ± 1.5
605 compared to untreated controls and an ANOVA-calculated significance level of $p < 0.01$ ($n = 3$).
606 (B) Significant probe changes identified using the described criteria are sorted by Venn diagram.

607

608 Figure 4. Venn diagram sorting identified unique genes regulated by co-exposure conditions at
609 both 4 and 24 h post-damage induction, and sorting of these uniquely regulated genes by time
610 point was performed.

611
612 Figure 5. DNA replication, recombination, and repair networks identified by IPA for the
613 uniquely regulated genes identified for the co-exposure condition 24 h after damage induction.
614 (A) DNA replication, recombination, and repair network 1 (score 46, 31 focus molecules, p value
615 of top functions 7.18E-05) is presented with expression values for the co-exposure overlaid, as
616 an indicator of up- or down-regulation (red and green, respectively). (B) DNA replication,
617 recombination, and repair network 3 (score 38, 28 focus molecules, p value of top functions
618 4.458E-08) is presented with expression values for the co-exposure overlaid, as an indicator of
619 up- or down-regulation (red and green, respectively).

620
621 Figure 6. Levels of chromatin condensation after treatment with KBrO₃, BPA, or co-exposure of
622 both agents at 4 and 24 h post-damage induction were measured by the Chromatin Condensation
623 & Membrane Permeability Dead Cell Apoptosis Kit (Life Technologies) using flow cytometry.
624 (A) Hoechst and PI stained live cells are sorted by intensity, and the contour maps of the
625 measured intensities for a representative experiment at 4 and 24 h are shown. Dashed line shows
626 the center of the control contour plot and highlights changes relative to the control cells. (B)
627 Mean intensities values of the Hoechst staining for each treatment condition 4 h post-damage
628 induction normalized to the control are shown (mean ± SEM of 3 biological replicates). (C)
629 Mean intensities of the Hoechst staining for each treatment condition 24 h post-damage
630 induction normalized to the control are shown (mean ± SEM). * $p < 0.05$, with solid and dashed
631 lines showing comparison groups.

632

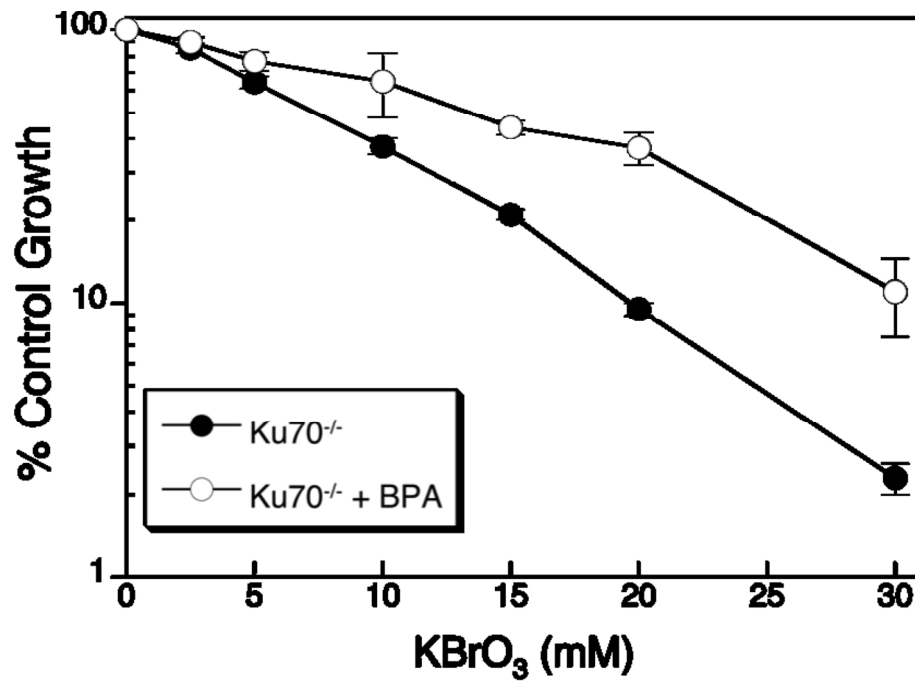
633 Figure 7. Levels of free GSH after treatment with KBrO_3 , BPA, or co-exposure of both agents at
634 4 and 24 h post-damage induction were measured by staining live cells with ThiolTracker Violet
635 and sorting by flow cytometry. (A) ThiolTracker Violet live cells are sorted by intensity and the
636 measured intensities for a representative experiment at 4 and 24 h are shown. Dashed line
637 indicated the center of the intensity peak for the control cells and highlights the relative changes
638 in measured intensity compared to the control cells. (B) Mean intensities values of the
639 ThiolTracker Violet staining for each treatment condition 4 h (black) and 24 h (red) after damage
640 induction normalized to the control are shown (mean \pm SEM of 3 replicates).

641

642 Figure 8. Time-line for the changes observed after BPA exposure. The initial exposure period, up
643 to 4 h post-damage induction, reveals a repression of DNA repair at both the recognition and
644 excision level and at the transcription level. Between 4 and 24 h an adaptive response is induced
645 by BPA co-exposure that results in the up-regulation of DNA repair networks, while alterations
646 in the cellular microenvironment are being induced through pH changes and anti-oxidant
647 depletion. These changes may result in long-term epigenetic changes or reprogramming events
648 that require further investigation.

649

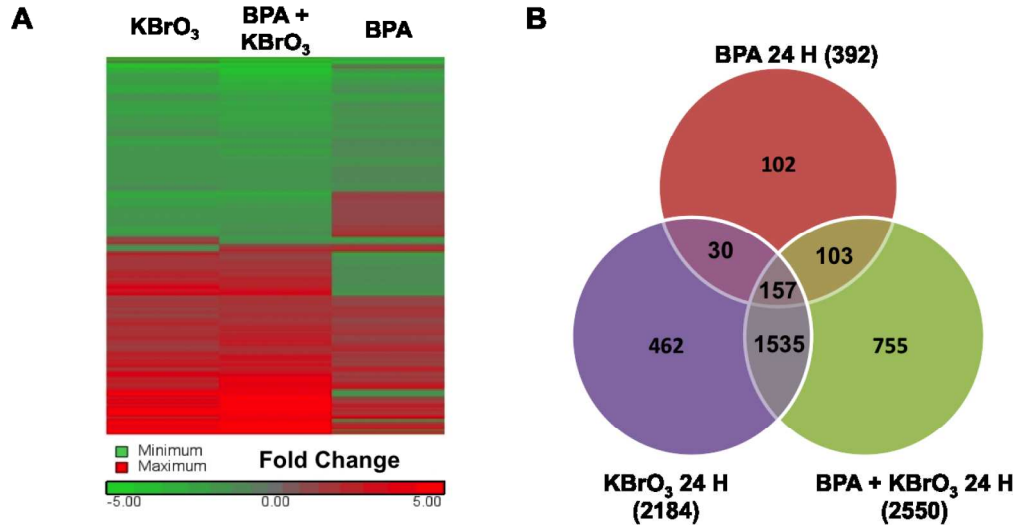
Figure 1



Cell survival following co-exposure of BPA and KBrO₃ from (Gassman et al. 2015). Ku70-deficient cells were treated with increasing amounts of KBrO₃ for 1 h (solid circles) or pre-treated with 150 μ M BPA for 1 h, co-exposed with BPA and increasing amounts of KBrO₃ for 1 h, then BPA exposure was continued for a total of 24 h (open circles), as described in (Gassman et al. 2015).

155x127mm (300 x 300 DPI)

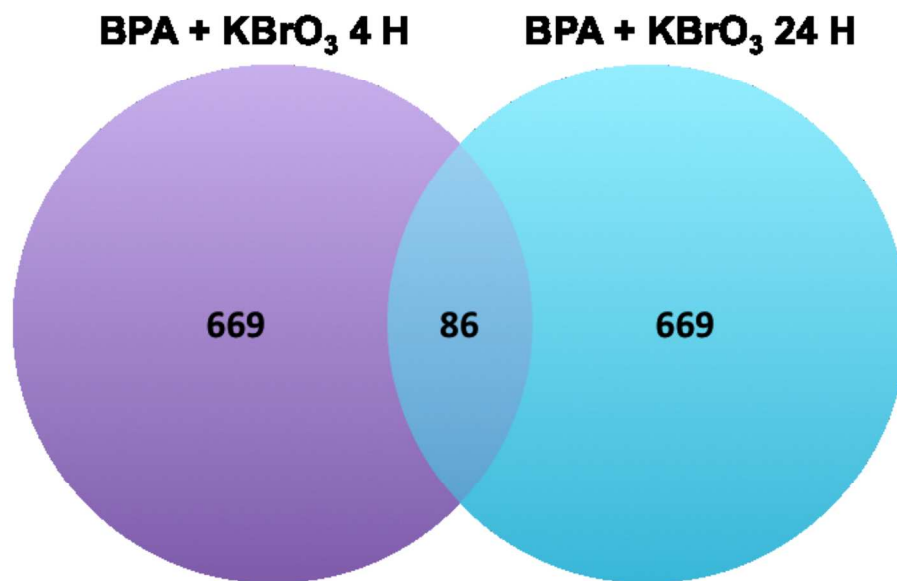
Figure 3



Gene expression changes observed by whole genome analysis of mRNA isolated 24 h after treatment with KBrO₃, BPA, or co-exposure of both agents, as described in Material and Methods. (A) Heat map of gene expression changes observed after treatment was generated using Partek® Genomic Suite software with probes selected by a fold-change cutoff of ± 1.5 compared to untreated controls and an ANOVA-calculated significance level of $p < 0.01$ ($n = 3$). (B) Significant probe changes identified using the described criteria are sorted by Venn diagram.

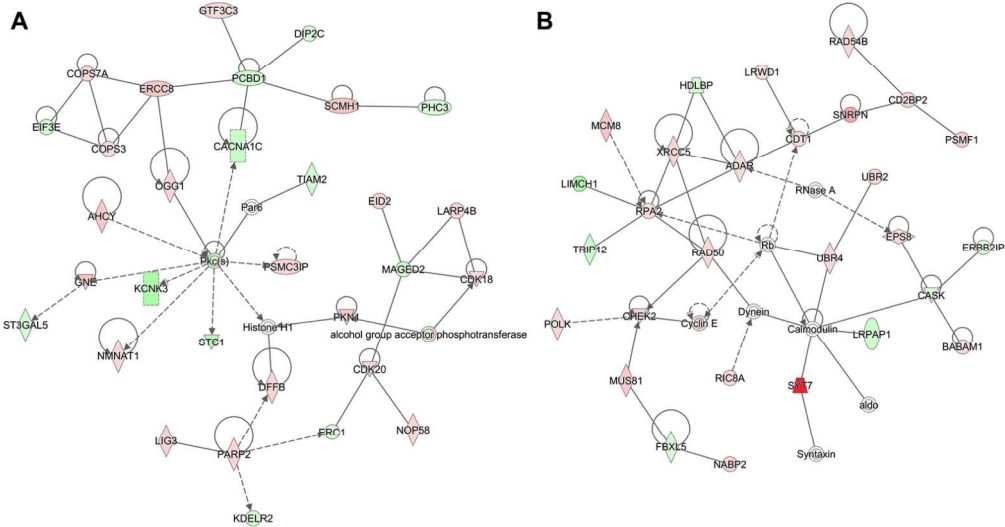
211x123mm (300 x 300 DPI)

Figure 4



Venn diagram sorting identified unique genes regulated by co-exposure conditions at both 4 and 24 h post-damage induction, and sorting of these uniquely regulated genes by time point was performed.
126x89mm (300 x 300 DPI)

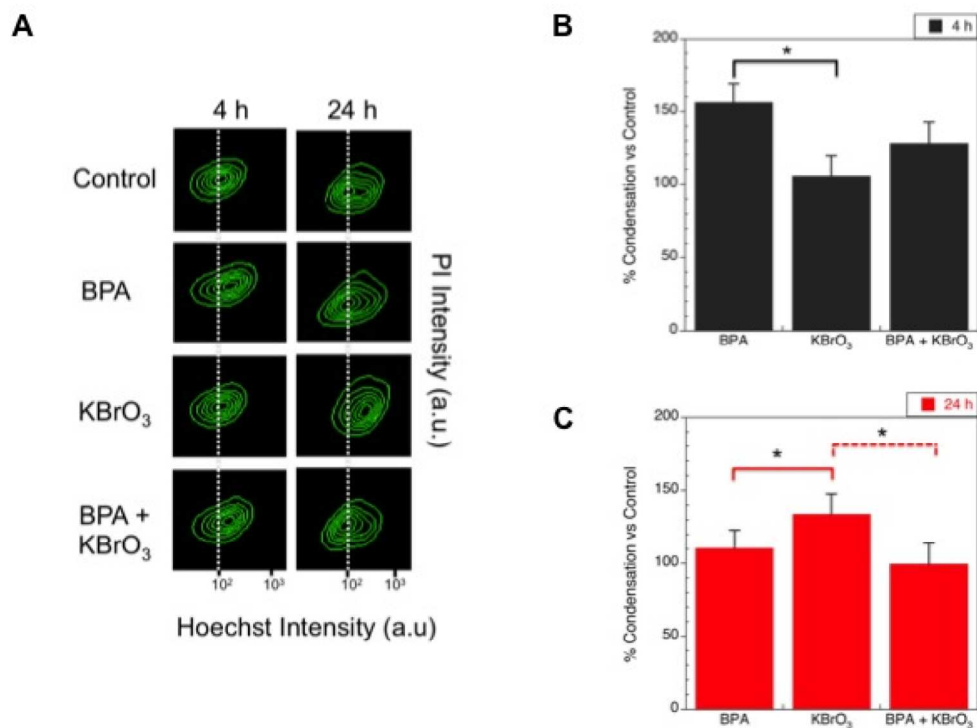
Figure 5



DNA replication, recombination, and repair networks identified by IPA for the uniquely regulated genes identified for the co-exposure condition 24 h after damage induction. (A) DNA replication, recombination, and repair network 1 (score 46, 31 focus molecules, p value of top functions 7.18E-05) is presented with expression values for the co-exposure overlaid, as an indicator of up- or down-regulation (red and green, respectively). (B) DNA replication, recombination, and repair network 3 (score 38, 28 focus molecules, p value of top functions 4.458E-08) is presented with expression values for the co-exposure overlaid, as an indicator of up- or down-regulation (red and green, respectively).

502x279mm (300 x 300 DPI)

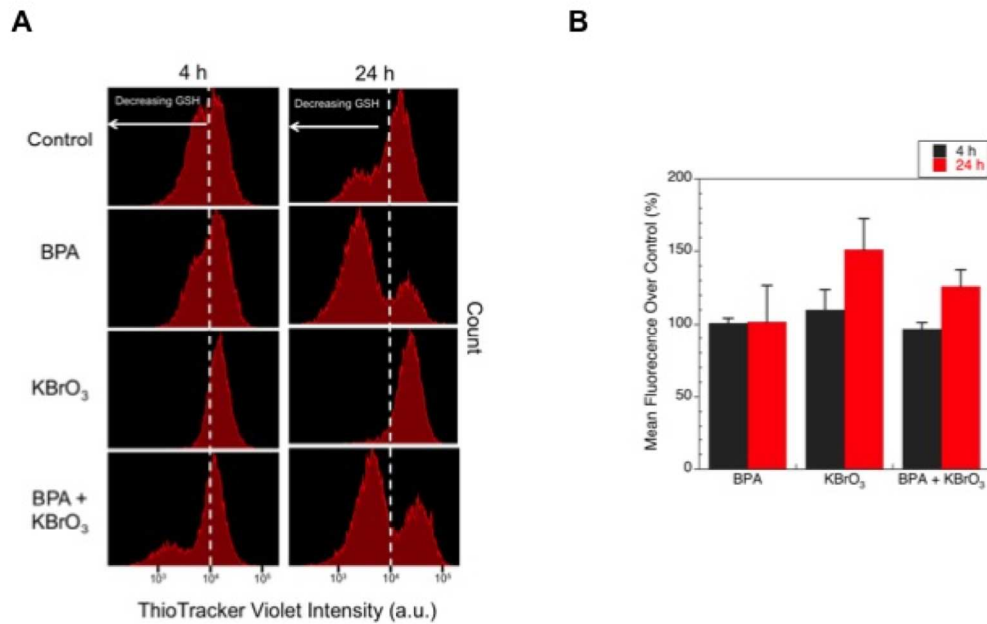
Figure 6



Levels of chromatin condensation after treatment with KBrO₃, BPA, or co-exposure of both agents at 4 and 24 h post-damage induction were measured by the Chromatin Condensation & Membrane Permeability Dead Cell Apoptosis Kit (Life Technologies) using flow cytometry. (A) Hoechst and PI stained live cells are sorted by intensity, and the contour maps of the measured intensities for a representative experiment at 4 and 24 h are shown. Dashed line shows the center of the control contour plot and highlights changes relative to the control cells. (B) Mean intensities values of the Hoechst staining for each treatment condition 4 h post-damage induction normalized to the control are shown (mean \pm SEM of 3 biological replicates). (C) Mean intensities of the Hoechst staining for each treatment condition 24 h post-damage induction normalized to the control are shown (mean \pm SEM of 3 replicates). * $p < 0.05$, with solid and dashed lines showing comparison groups.

211x166mm (300 x 300 DPI)

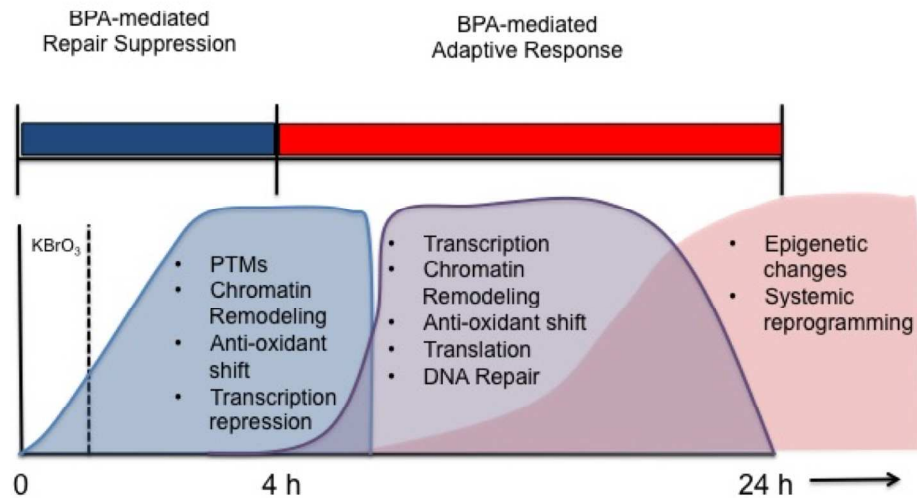
Figure 7



Levels of free thiols (GSH) after treatment with KBrO₃, BPA, or co-exposure of both agents at 4 and 24 h post-damage induction were measured by staining live cells with ThioTracker Violet and sorting by flow cytometry. (A) ThioTracker Violet live cells are sorted by intensity and the measured intensities for a representative experiment at 4 and 24 h are shown. Dashed line indicated the center of the intensity peak for the control cells and highlights the relative changes in measured intensity compared to the control cells. (B) Mean intensities values of the ThioTracker Violet staining for each treatment condition 4 (black) and 24 h (red) post-damage induction normalized to the control are shown (mean ± SEM of 3 replicates).

217x147mm (300 x 300 DPI)

Figure 8



Time-line for the changes observed after BPA exposure. The initial exposure period, up to 4 h post-damage induction, reveals a repression of DNA repair at both the recognition and excision level and at the transcription level. Between 4 and 24 h an adaptive response is induced by BPA co-exposure that results in the up-regulation of DNA repair networks, while alterations in the cellular microenvironment are being induced through pH changes and anti-oxidant depletion. These changes may result in long-term epigenetic changes or reprogramming events that require further investigation.

223x132mm (300 x 300 DPI)